[11] C.-F. Cheng, W. Zhou, J. Klinowski, *Chem. Phys. Lett.* **1996**, *263*, 247.
[12] A. Corma, Q. Kan, M. T. Navarro, J. Perez-Pariente, F. Rey, *Chem. Mater.* **1997**, *9*, 2123.
[13] M. Kruk, M. Jaroniec, A. Sayari, *J. Phys. Chem. B* **1999**, *103*, 4590.
[14] A. Sayari, *Angew. Chem. Int. Ed.* **2000**, *39*, 2920.
[15] J. M. Kim, G. D. Stucky, *Chem. Commun.* **2000**, 1159.
[16] S.-S. Kim, T. R. Pauly, T. J. Pinnavaia, *Chem. Commun.* **2000**, 1661.
[17] P. T. Tanev, T. J. Pinnavaia, *Chem. Mater.* **1996**, *8*, 2068.
[18] R. Mokaya, W. Zhou, W. Jones, *Chem. Commun.* **1999**, 51.
[19] R. Mokaya, *J. Phys. Chem. B* **1999**, *103*, 10 204.
[20] R. Mokaya, W. Zhou, W. Jones, *J. Mater. Chem.* **2000**, *10*, 1139.
[21] K. W. Gallis, C. C. Landry, *Chem. Mater.* **1997**, *9*, 2035.
[22] A. Sayari, M. Kruk, M. Jaroniec, *Catal. Lett.* **1997**, *49*, 147.
[23] M. Kruk, M. Jaroniec, A. Sayari, *Microporous Mesoporous Mater.* **1999**, *29*, 217.
[24] Q. Huo, D. I. Margolese, U. Ciesla, P. Feng, T. E. Gier, P. Sieger, R. Leon, P. M. Petroff, F. Schuth, G. D. Stucky, *Nature* **1994**, *368*, 317.
[25] D. Zhao, Q. Huo, J. Feng, B. F. Chmelka, G. D. Stucky, *J. Am. Chem. Soc.* **1998**, *120*, 6024.
[26] J.-H Sun, Z. Shan, J. A. Moulijn, J. C. Jansen, T. Maschmeyer, M.-O. Coppens, unpublished.
[27] J. C. P. Broekhoff, J. H. de Boer, *J. Catal.* **1967**, *9*, 8. J. C. P. Broekhoff, J. H. de Boer, *J. Catal.* **1968**, *9*, 15.

General Route to Homogeneous, Mesoporous, Multicomponent Oxides Based on the Thermolytic Transformation of Molecular Precursors in Non-polar Media**

By *Joshua W. Kriesel*, *Melissa S. Sander*, and *T. Don Tilley**

The construction of nanostructured materials with tailored properties is a challenging goal that is widely regarded as representing a key first step toward new technologies.[1] This challenge has been met with significant advances in recent years, especially with the application of surfactants in the synthesis of mesoporous inorganic oxides.[2–17] In particular, this approach has demonstrated that a range of silica mesostructures with highly regular pore structures can be obtained.[2–6] However, these templating methods have been extended with sporadic success to analogous non-silica oxides and multi-component materials.[7–18] Clearly, synthetic methods that allow variations in the composition of nanostructured solids, and access to complex stoichiometries for such materials, would greatly increase the potential for technological applications.

The generation of complex stoichiometries is generally problematic in inorganic synthesis, especially for metastable and non-crystalline combinations of elements.[19] With regard to this problem we have developed a synthetic strategy, based on molecular-level control, for producing homogeneous (i.e., well-dispersed) multi-component oxides.[20] This route to inorganic oxides differs significantly from commonly employed solution methods, in that it utilizes non-polar solvents and results in inherently higher surface areas and greater elemental dispersities. Here, we report a general method for the synthesis of mesoporous, multi-component oxides (denoted UCB1), based on the use of several molecular precursors in conjunction with block copolymer templates. This method is illustrated for materials with the compositions $ZrO_2{\cdot}4SiO_2$, $Ta_2O_5{\cdot}6SiO_2$, $Fe_2O_3{\cdot}6SiO_2$, and $AlPO_4$.

Previously, we reported the use of single-source molecular precursors possessing $-OSi(O^tBu)_3$ and $-O(O)P(O^tBu)_2$ ligands in the synthesis of non-mesostructured homogeneous, mixed-element oxides under mild conditions.[20–22] These oxygen-rich, mixed-element precursors eliminate isobutylene and water at low temperature (90–150 °C), in the solid state or in solution. For example, we have prepared highly dispersed $ZrO_2{\cdot}4SiO_2$ by thermal decomposition of $Zr[OSi(O^tBu)_3]_4$ according to Equation 1.[20] Thus, all the elements that are incorporated into the material emanate from a single molecular species. The facile formation of carbon-free materials in this process may be attributed to the pre-existing oxygen environment for the precursor compounds.

$$Zr[OSi(O^tBu)_3]_4 \xrightarrow{\Delta} ZrO_2{\cdot}4SiO_2 + 12CH_2{=}CMe_2 + 6H_2O \quad (1)$$

In this work, mesostructured homogeneous mixed-element oxides were obtained by adding a toluene solution of a block polyalkylene oxide copolymer (e.g., $HO(CH_2CH_2O)_{106}$–$(CH_2CH(CH_3)O)_{70}(CH_2CH_2O)_{106}H$, abbreviated as EO_{106}-$PO_{70}EO_{106}$) to the molecular precursor. This mixture was sealed in an ampoule, heated at 135 °C for 12 h, and the resulting monolith was allowed to air dry. Thermal gravimetric analysis (TGA) of these mixed oxide/polymer containing materials revealed a precipitous weight loss of ca. 50 % with an onset temperature of ca 250 °C. This weight loss corresponds to efficient oxidative decomposition and removal of the block copolymer.[23] Polymer-free mesostructured mixed-element oxides (UCB1 materials; Table 1) were obtained by calcination of the polymer-containing gels at 500 °C for 3 h under O_2. Using this synthetic protocol, the molecular precursors $Zr[OSi(O^tBu)_3]_4$, $(EtO)_2Ta[OSi(O^tBu)_3]_3$, $Fe[OSi(O^tBu)_3]_3{\cdot}THF$ (THF = tetrahydrofuran), and $[Al(O^iPr)_2O_2P(O^t\text{-}Bu)_2]_4$ have been converted into the corresponding mesostructured materials $ZrO_2{\cdot}4SiO_2$, $1/2Ta_2O_5{\cdot}3SiO_2$, $1/2Fe_2O_3{\cdot}3SiO_2$, and $AlPO_4$ (denoted UCB1–ZrSi, UCB1–TaSi, UCB1–FeSi, UCB1–AlP, respectively). The template-directed synthesis of mixed-element oxides in non-polar media is particularly notable since previous reports on the preparation of mesoporous oxide materials describe synthetic protocols that employ polar (usually aqueous) solvents.[2–18] Presumably, this is due to the fact that these procedures entail the hydrolysis of metal species and utilize the solvent-mediated self-assembly of amphiphilic templates, in conjunction with electrostatic and hydrogen bonding forces.

[*] Prof. T. D. Tilley,[+] M. S. Sander,[+] J. W. Kriesel[+]
Department of Chemistry
University of California, Berkeley
Berkeley, CA 94720-1460 (USA)
E-mail: tdtilley@socrates.berkeley.edu
[+] Second address: Chemical Sciences Division, Lawrence Berkeley National Laboratory, 1 Cyclotron Road, Berkeley, CA 94720, USA.

[**] This work was supported by the Director, Office of Basic Energy Sciences, Chemical Sciences Division, of the US Department of Energy under Contract No. DE-AC03-76SF00098. We thank Drs. Kevin Ott and Andrea Labouriau for the acquisition of solid state NMR spectra and are grateful to Chris Nelson at the National Center for Electron Microscopy for technical assistance.

  0935-9648/01/0503-0331 $ 17.50+.50/0

ADVANCED MATERIALS

All UCB1 materials exhibit a single peak in the low angle powder X-ray diffraction (XRD) spectrum (Table 1). The absence of higher angle peaks indicates that the inorganic walls of these materials are amorphous. Typical XRD patterns for UCB1 materials, illustrated for UCB1–TaSi and UCB1–ZrSi, are shown in Figure 1. Although these single-peak XRD patterns are an indication of a lack of long-range order, they suggest the presence of a disordered hexagonal[3] or wormhole-type pore structure.[24] As shown in Table 1, the ordering lengths of the UCB1 materials are 102–113 Å.

A more detailed description of the mesoscopic order in UCB1 materials was obtained by transmission electron microscopy (TEM). All the UCB1 materials reported in Table 1 exhibit wormhole-like pore structures with no apparent long-range order, as illustrated in the micrograph of UCB1–ZrSi (Fig. 2). Pores in the UCB1 materials presumably originate from the space previously occupied by polymer assemblies. However, despite the lack of long-range order, these materials possess relatively uniform channel spacings. For comparison, a TEM image of $ZrO_2{\cdot}4SiO_2$ obtained from $Zr[OSi(O^tBu)_3]_4$ without the addition of a polymeric template is shown in Figure 2b. Thus, untemplated $ZrO_2{\cdot}4SiO_2$ exhibits textural mesoporosity, in which the voids are defined by the packing of different-sized particles. Conversely, the porosity in UCB1–ZrSi appears to result from the mesoscale ordering of the material's framework structure.

Porosity in the UCB1 materials was further characterized using nitrogen porosimetry. The N_2 adsorption–desorption isotherms for all the UCB1 materials reported in Table 1 are type IV curves with H1 or H2 hystereses.[25] For example, UCB1–AlP exhibits an N_2 isotherm (Fig. 3) that features a steep rise in adsorption between relative pressures (P/P_0) of 0.6–0.8, with no additional adsorption at $P/P_0 > 0.8$. Similarly, all the UCB1–ZrSi materials display N_2 isotherms with no adsorption above $P/P_0 = 0.6$. The lack of adsorption at high relative pressures indicates that there is little textural mesoporosity in the UCB1 materials. Instead, the N_2 isotherms for these materials indicate framework-confined mesoporosity in which the pores arise from templated framework channels, and therefore corroborate the TEM analysis.[26]

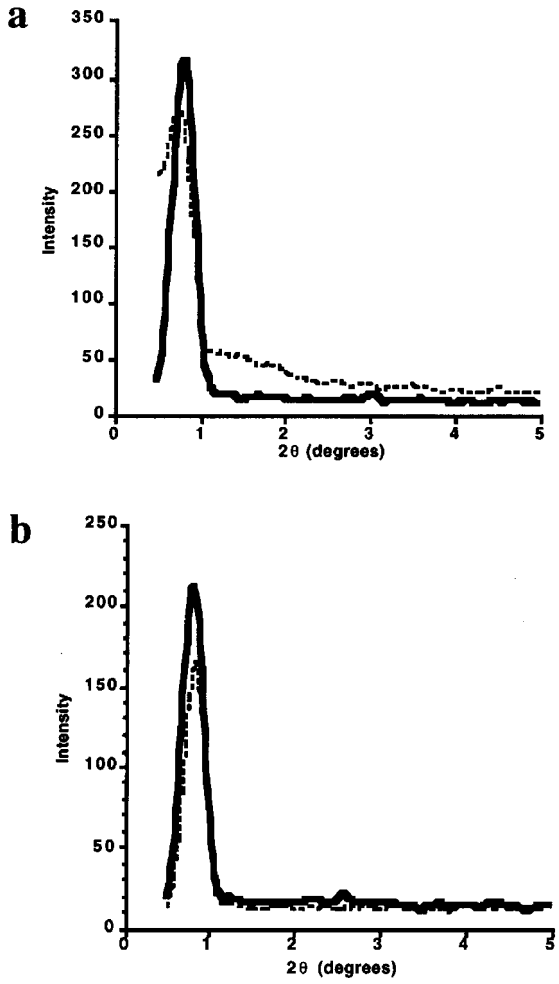

Fig. 1. Powder XRD patterns of UCB1–TaSi (a) and UCB1–ZrSi (b). The dotted lines are patterns of the as-made oxide–polymer composite mesostructures. The solid lines are patterns of the calcined UCB1 materials.

Table 1. The N_2 porosimetry and XRD data for the UCB1 materials. The corresponding untemplated materials are shown for comparison.

Oxide	Precursor	Template	UCB#	Surf. area [m^2/g]	Pore rad. [Å]	d_{100} [Å]	Wall thick. [Å]	Pore vol. [cc/g]
$ZrO_2{\cdot}4SiO_2$	$Zr[OSi(O^tBu)_3]_4$	NONE	-	555	112	-	-	1.00
$ZrO_2{\cdot}4SiO_2$	$Zr[OSi(O^tBu)_3]_4$	$EO_{106}PO_{70}EO_{106}$	UCB1-ZrSi	540	22	110	66	0.42
$ZrO_2{\cdot}4SiO_2$	$Zr[OSi(O^tBu)_3]_4$	$EO_{20}PO_{70}EO_{20}$	UCB1-ZrSi	545	20	111	71	0.45
$ZrO_2{\cdot}4SiO_2$	$Zr[OSi(O^tBu)_3]_4$	$EO_{20}PO_{30}EO_{20}$	UCB1-ZrSi	490	13	110	84	0.35
$ZrO_2{\cdot}4SiO_2$	$Zr[OSi(O^tBu)_3]_4$	$EO_{13}PO_{30}EO_{13}$	UCB1-ZrSi	560	13	100	74	0.43
$ZrO_2{\cdot}4SiO_2$	$Zr[OSi(O^tBu)_3]_4$	$H_{33}C_{16}(OCH_2CH_2)_{10}OH$	UCB1-ZrSi	530	16	113	81	0.41
$Ta_2O_5{\cdot}6SiO_2$	$(EtO)_2Ta[OSi(O^tBu)_3]_3$	NONE	-	415	34	-	-	0.71
$Ta_2O_5{\cdot}6SiO_2$	$(EtO)_2Ta[OSi(O^tBu)_3]_3$	$EO_{106}PO_{70}EO_{106}$	UCB1-TaSi	400	19	106	68	0.41
$Ta_2O_5{\cdot}6SiO_2$	$(EtO)_2Ta[OSi(O^tBu)_3]_3$	$EO_{20}PO_{70}EO_{20}$	UCB1-TaSi	440	19	110	72	0.44
$AlPO_4$	$(^iPrO)_2AlO_2P(O^tBu)_2$	NONE	-	360	61	-	-	1.10
$AlPO_4$	$(^iPrO)_2AlO_2P(O^tBu)_2$	$EO_{106}PO_{70}EO_{106}$	UCB1-AlP	670	39	111	33	1.13
$AlPO_4$	$(^iPrO)_2AlO_2P(O^tBu)_2$	$EO_{20}PO_{70}EO_{20}$	UCB1-AlP	750	33	113	47	1.11
$Fe_2O_3{\cdot}6SiO_2$	$Fe[OSi(O^tBu)_3]_3{\cdot}THF$	NONE	-	520	25	-	-	0.69
$Fe_2O_3{\cdot}6SiO_2$	$Fe[OSi(O^tBu)_3]_3{\cdot}THF$	$EO_{106}PO_{70}EO_{106}$	UCB1-FeSi	400	12	102	80	0.34
$Fe_2O_3{\cdot}6SiO_2$	$Fe[OSi(O^tBu)_3]_3{\cdot}THF$	$EO_{20}PO_{70}EO_{20}$	UCB1-FeSi	355	17	105	71	0.34

The Barrett–Joyner–Halenda (BJH) analysis of the adsorption branch of the isotherms for all the UCB1 materials indicates narrow pore size distributions (see Fig. 3). As shown in Table 1, pore radii for the silica-containing UCB1 materials ranged from 12–22 Å, depending on the block copolymer employed. Additionally, the surface areas and

  0935-9648/01/0503-0332 $ 17.50+.50/0

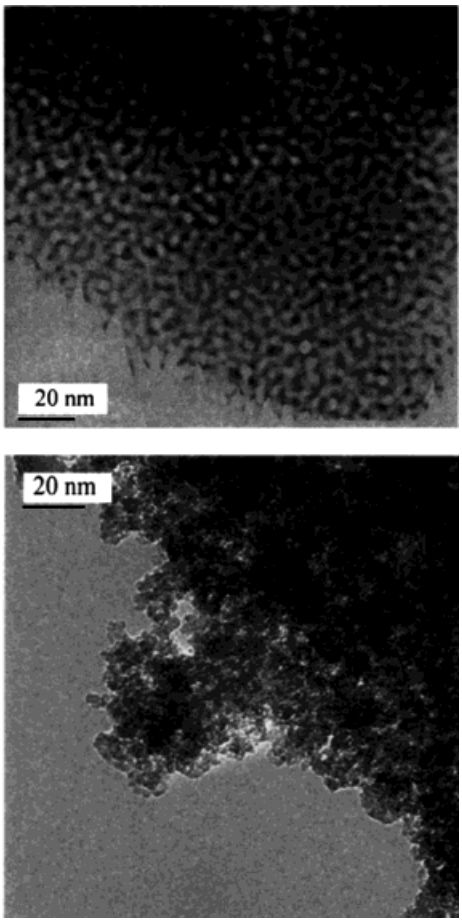

Fig. 2. TEM images of a) UCB1–ZrSi prepared using $(H_{33}C_{16})_{10}(OCH_2CH_2)_{10}OH$ block copolymer, and of b) $ZrO_2{\cdot}4SiO_2$ prepared without the addition of a polymeric template. Both samples had been previously calcined to 500 °C under O_2.

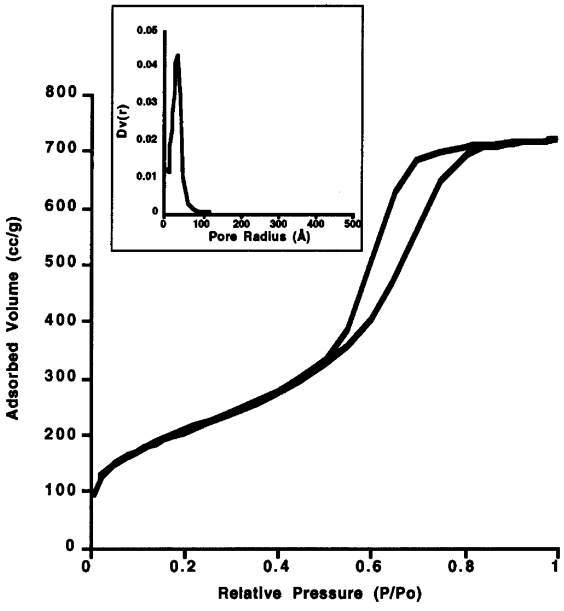

Fig. 3. The N_2 isotherm for a UCB1–AlP material prepared using the $EO_{20}PO_{70}EO_{20}$ triblock copolymer template. The corresponding BJH pore size distribution, shown in the inset, was calculated from the adsorption branch of the isotherm.

pore volumes of these materials are quite large relative to other templated mixed-element oxides (50–200 m^2/g).[7] BJH analyses of the UCB1–AlP materials revealed large mesopores with radii of 33 and 39 Å, which correlate with the length of the block copolymer employed (see Table 1). The pore radii of the UCB1–AlP materials are significantly larger than those reported for other mesostructured $AlPO_4$ materials (10–18 Å).[17] The UCB1–AlP materials also have a particularly well-defined N_2 isotherm, as is evident by observation of two distinct adsorption processes: i) monolayer coverage and ii) capillary condensation ($P/P_0 \approx 0.6$). These materials have a somewhat higher surface area and larger pore diameters than the other UCB materials (see Table 1). The reason for this is currently not clear, but it suggests that the aluminum phosphate network is less prone to collapse during the dessication and calcination process. Note that the mesoporous UCB1–AlP materials are of particular interest as new modifications of aluminophosphates, which have been widely studied for their catalytic and ion exchange properties.[17,18]

Because the UCB1 materials possess fairly narrow pore size distributions and have relatively uniform channel spacings, an estimate of the wall thickness can be obtained by assuming that the observed *d*-spacing corresponds to a channel-to-channel distance.[27] Thus, using the XRD and pore size data, the wall thickness of the silica-containing UCB1 materials was determined to be 66–84 Å, and 33–47 Å for the UCB1–AlP materials. The framework walls of the mixed-element oxides reported in Table 1 are significantly thicker than those for MCM-41 silicas (10–15 Å)[2] and thicker than those of previously reported mixed-element oxides templated in aqueous solution by triblock copolymers (35–40 Å).[7]

A key distinguishing property expected for the molecular precursor-derived UCB1 materials is the composition of the inorganic framework, and a related issue concerns the dispersion of inorganic components. Energy dispersive X-ray spectroscopy (EDX) was employed to assess the stoichiometry of the various samples. EDX spectra taken from large (ca. 100 nm) areas showed the expected elemental ratios in all the UCB1 materials, within the experimental error of this technique. Additionally, local EDX spectroscopy was used to probe the distribution of elements in the inorganic framework at high spatial resolution (1 nm). For example, the EDX profile of UCB1–ZrSi (Fig. 4) provides a measure of the relative amounts of Zr and Si at 1 nm resolution, along a 350 nm section of the sample (ca. 3.5 nm acquisition intervals). The intensities of the points for both Zr and Si increase over the sampling length due to a steady increase in the thickness of the material. As shown in the inset of Figure 4, the EDX profile shows the expected Si/Zr ratio (over the entire sample region) in this $ZrO_2{\cdot}4SiO_2$ material, and provides evidence for a uniform dispersion of elements in the inorganic framework.

Further indications of homogeneity in the UCB1 materials were obtained from their crystallization behavior at high temperature. For multi-component oxides there is often a correlation between sample homogeneity and the temperature at which a single component metal oxide phase separates from

  0935-9648/01/0503-0333 $ 17.50+.50/0

ADVANCED MATERIALS

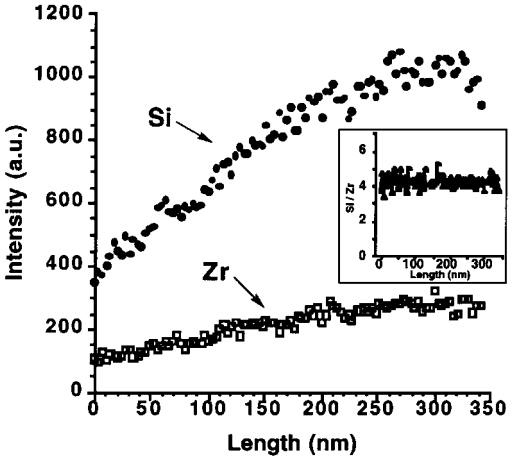

Fig. 4. An EDX profile of UCB1–ZrSi performed using a 10 Å probe at 35 Å intervals (8 s/pt). Points shown as ● and □ correspond to Si and Zr, respectively. The error in these intensities is estimated to be ≤10 %. The inset shows the ratio of Si/Zr at each point along the profile.

the material, and subsequently, crystallizes. In ZrO_2–SiO_2, Ta_2O_5–SiO_2 and Fe_2O_3–SiO_2 systems, a delayed crystallization of a transition metal oxide phase indicates the presence of an atomically well-mixed multi-component oxide.[28–30] UCB1–ZrSi is amorphous until 1100 °C (2 h, under O_2), when nano-sized tetragonal zirconia (t-ZrO_2) crystallites are first observed (by XRD). Additionally, delayed crystallization in UCB1–TaSi was observed with formation of nanocrystalline L-Ta_2O_5 after heating at 1100 °C. Finally, UCB1–FeSi materials are amorphous until 1000 °C, at which time α-Fe_2O_3 crystallites are visible by powder XRD.

Further characterization of the UCB1–AlP materials by ^{27}Al cross polarization magic angle spinning nuclear magnetic resonance (CP MAS NMR) spectroscopy revealed an intense peak at 42 ppm and a weaker resonance at –11 ppm. The downfield resonance corresponds to tetrahedrally coordinated Al in an AlO_4 structural unit.[31] Octahedrally coordinated Al, arising from structural units of the type $Al(OP)_4(OH_2)_2$, most likely gives rise to the resonance at ca. –11 ppm.[31] The ^{31}P MAS NMR spectrum contains a single peak at –25 ppm, which can be attributed to $P(OAl)_4$ tetrahedra and is outside the range for P–O–P linkages.[16,31] Thus, the UCB1–AlP framework appears to be built primarily of Al–O–P heterolinkages.

The thermal and hydrothermal stabilities of the UCB1 materials are very high. For example, after boiling UCB1–ZrSi in water at reflux for 48 h, there was no change in the value of the low-angle XRD peak and only a small loss in surface area (32 %). Aditionally, calcination of UCB1–ZrSi, UCB1–TaSi, UCB1–FeSi, and UCB1–AlP at 800 °C under O_2 for 2 h led to surprisingly small reductions in surface areas (20, 26, 31, and 53 %, respectively) and did not destroy the mesoscopic order in the gels, as determined by XRD and N_2 porosimetry. The preservation of significant mesoscopic order in these materials after treatment to very high temperature probably reflects the presence of the thick framework walls. The thermal stability of UCB1–AlP is particularly notable since many of the $AlPO_4$–surfactant composites reported to date are not thermally stable and incur loss of mesoscopic order under relatively mild conditions.[17]

Previous reports on template assisted mesoporous metal oxide formation describe synthetic protocols that employ highly polar (usually aqueous) reaction solvents.[2–18] This synthetic approach is rational, given that poly(alkylene oxide) block copolymers are known to self-assemble into well defined mesophases in aqueous media.[32] In addition, polar solvents are expected to play an important role in mesoporous oxide formation, in that they are expected to facilitate cooperative assembly of the template and inorganic species via electrostatic and hydrogen bonding interactions.[7] Very little is known concerning the phase behavior of poly(alkylene oxide) block copolymers in non-aqueous solvents;[32] however, the observation described here concerning formation of the mesostructured UCB1 materials in a non-polar environment would seem to have important implications for the synthesis of nanostructured materials. In this context, we are currently investigating the mechanism of formation of the materials reported here.

In conclusion, we have demonstrated a new general route to mesoporous mixed-element oxides with high surface areas, homogenous dispersions of elements and thick framework walls. We anticipate that this molecular precursor route will allow us to access a wide range of materials with more complex compositions and intricate nanoarchitectures, which may be useful in applications such as catalysis and electronic materials.

Experimental

A typical preparation for the mesoporous oxides reported herein is illustrated for UCB1–ZrSi. 0.20 g of the block copolymer was dissolved in 6.0 mL of dry toluene. After the polymer fully dissolved, the solution was transferred to a glass tube that was interfaced through a Cajon adapter to a glass fitting with an N_2 inlet and septum, containing 0.60 g of $Zr[OSi(O^tBu)_3]_4$. This mixture was freeze-pump-thawed at least 4 times and then sealed with a torch under vacuum. The glass ampoule was then placed in an oven that was preheated to 135 °C and heated overnight. Typical gel times were 3–24 h. Adding a catalytic amount of $AlCl_3$ (ca. 0.5 mg) significantly reduced gel times, but seemed to have no effect on the properties of UCB1–ZrSi. The monolith was isolated by opening the ampoule and allowing the gel to air dry in a Petri dish for 3–5 d at room temperature, after which time the gel had shrunk by ca. 70 % and cracked into several pieces. The gel was then powdered and calcined at 500 °C under O_2 in a tube furnace for 3 h. EDX Si/Zr anal. found for UCB1–ZrSi: Si = 81, Zr = 19. Anal found for C and H: C, <0.2; H, 1.66.

Received: September 5, 2000
Final version: November 6, 2000

[1] S. I. Stupp, V. LeBonheur, K. Walker, L. S. Li, K. E. Huggins, M. Keser, A. Amstutz, *Science* **1997**, *276*, 384.
[2] C. T. Kresge, M. E. Leonowicz, W. J. Roth, J. C. Vartuli, J. S. Beck, *Nature* **1992**, *359*, 710.
[3] S. A. Bagshaw, E. Prouzet, T. J. Pinnavaia, *Science* **1995**, *269*, 1242.
[4] T. Yanagisawa, T. Shimizu, K. Kuroda, C. Kato, *Bull. Chem. Soc. Jpn.* **1990**, *63*, 988.
[5] K. M. McGrath, D. M. Dabbs, N. Yao, A. Aksay, S. M. Gruner, *Science* **1997**, *277*, 552.
[6] D. Zhao, J. Feng, Q. Huo, N. Melosh, G. H. Fredrickson, B. F. Chmelka, G. D. Stucky, *Science* **1998**, *279*, 548.
[7] P. Yang, D. Zhao, D. I. Margolese, B. F. Chmelka, G. D. Stucky, *Nature* **1998**, *396*, 152.

  0935-9648/01/0503-0334 $ 17.50+.50/0

[8] M. Templin, A. Franck, A. D. Chesne, H. Leist, Y. Zgang, R. Ulrich, U. Schadler, U. Wiesner, *Science* **1997**, *278*, 1795.
[9] A. Sayari, P. Liu, *Microporous Mater.* **1997**, *12*, 149.
[10] D. M. Antonelli, J. Y. Ying, *Chem. Mater.* **1996**, *8*, 874.
[11] S. A. Bagshaw, T. J. Pinnavaia, *Angew. Chem. Int. Ed. Engl.* **1996**, *35*, 1102.
[12] M. S. Wong, J. Y. Wong, *Chem. Mater.* **1998**, *10*, 2067.
[13] Z. Tian, W. Tong, J. Wang, N. Duan, V. V. Krishnan, S. L. Suib, *Science* **1997**, *276*, 926.
[14] S. A. Bagshaw, T. Kemmitt, N. B. Milestone, *Microporous Mesoporous Mater.* **1998**, *22*, 419.
[15] D. Khushalani, O. Dag, G. A. Ozin, A. Kuperman, *J. Mater. Chem.* **1999**, *9*, 1491.
[16] B. T. Holland, P. K. Isbester, C. F. Blanford, E. J. Munson, A. Stein, *J. Am. Chem. Soc.* **1997**, *119*, 6796.
[17] T. Kimura, Y. Sugahara, K. Kuroda, *Microporous Mesoporous Mater.* **1998**, *22*, 115.
[18] U. Ciesla, M. Früba, G. D. Stucky, F. Schöth, *Chem. Mater.* **1999**, *11*, 227.
[19] C. J. Brinker, G. W. Scherer, *Sol–Gel Science: The Physics and Chemistry of Sol–Gel Processing*, Academic, San Diego, CA **1990**.
[20] K. W. Terry, C. G. Lugmair, T. D. Tilley, *J. Am. Chem. Soc.* **1997**, *119*, 9745.
[21] C. G. Lugmair, *Ph.D. Thesis*, University of California at Berkeley **1997**.
[22] C. G. Lugmair, T. D. Tilley, A. L. Rheingold, *Chem. Mater.* **1999**, *11*, 1615.
[23] Q. Huo, D. I. Margolese, U. Ciesla, D. G. Demuth, P. Feng, T. E. Gier, P. Sieger, A. Firouzi, B. F. Chmelka, G. D. Stucky, *Chem. Mater.* **1994**, *6*, 1176.
[24] T. R. Pauly, Y. Liu, T. J. Pinnavaia, S. J. L. Billinge, T. P. Rieker, *J. Am. Chem. Soc.* **1999**, *121*, 8835.
[25] S. J. Gregg, K. S. W. Sing, *Adsorption, Surface Area and Porosity*, 2nd ed., Academic, London **1982**.
[26] P. T. Tanev, T. J. Pinnavaia, *Chem. Mater.* **1996**, *8*, 2068.
[27] E. Prouzet, T. J. Pinnavaia, *Angew. Chem. Int. Ed. Engl.* **1997**, *36*, 516.
[28] G. Guiu, P. Grange, *Bull. Chem. Soc. Jpn.* **1994**, *67*, 2716.
[29] J. B. Miller, E. I. Ko, *Catal. Today* **1997**, *35*, 269.
[30] G. Ennas, A. Musinu, G. Piccaluga, D. Zedda, D. Gatteschi, C. Sangregorio, J. L. Stanger, G. Concas, G. Spano, *Chem. Mater.* **1998**, *10*, 495.
[31] G. E. Engelhardt, D. Michel, *High-Resolution Solid-State NMR of Silicates and Zeolites*, Wiley, New York **1987**.
[32] B. Chu, Z. Zhou, in *Nonionic Surfactants: Polyalkylene Block Copolymers* (Ed: V. M. Nace), Surfactant Sci. Ser., Vol. 60, Marcel Dekker, New York **1996**.

Molecular Identification by Time-Resolved Interferometry in a Porous Silicon Film**

By *Sonia E. Létant*, and *Michael J. Sailor**

Porous silicon (PSi) is a nanocrystalline material that is generated by etching of bulk crystalline silicon in aqueous hydrofluoric acid (HF). It is of interest for its luminescence,[1] electroluminescence,[2] and sensor properties.[3] The open pore structure and large specific surface area (a few hundred m^2 per cm^3, corresponding to about a thousand times the surface of a polished silicon wafer) make porous Si a convenient material for sensitive detection of liquid and gaseous analytes. The ability to electrochemically tune the pore diameters[4] and to chemically modify the surface[5–7] provides control over the size and type of molecules adsorbed. These properties have been exploited to develop porous Si sensors for detection of toxic gases,[8,9] solvents,[10–12] explosives,[13,14] DNA,[15,16] and proteins.[4,17] The main techniques investigated to achieve signal transduction are capacitance,[18] resistance,[19] photoluminescence,[20] and reflectivity.[21] Detection limits of at least a few ppb have been demonstrated for some of these.[3] Nevertheless, no work has appeared concerning the use of porous Si matrices for the analysis of mixtures of chemical compounds.

The aim of this study was to determine whether or not time-resolved reflectivity measurements on porous Si films can be used to discriminate constituents of a binary gas mixture. Snow and co-workers[11] measured a time of stabilization of the reflectivity signal from a porous Si Bragg reflector exposed to chlorobenzene vapor to be 240 s and suggested that the data contained information on the adsorption dynamics. We confirm this, using a chemically modified single layer porous Si interferometer and a mixture of acetone and ethanol. The time evolution of the reflectivity signal immediately after exposure to a condensable analyte is expected to depend on the kinetics of diffusion, adsorption and capillary condensation of the analyte in the nanoporous matrix. It provides an ability to discriminate or identify individual components of a mixture similar to a chromatographic experiment.

Porous Si samples were electrochemically etched from monocrystalline p-type silicon substrates (boron-doped, ~0.001 Ω cm, (100) oriented, from Siltronix Inc.), at a current density of 50 mA/cm^2, in a 3:1 v/v mixture of aqueous HF (49% hydrofluoric acid, Fisher Scientific Chemicals Inc.) and ethanol (Fisher Chemicals Inc.). The samples were oxidized in a stream of ozone (OZOMAX 3, flux of 8 g/h) for 20 min prior to mounting in a gas exposure chamber. Fourier transform infrared (FTIR) spectra[17] show that this treatment removes the initial silicon hydride coverage (Si–H_x, with x=1,2,3, stretching bands around 2100 cm^{-1}) and forms silicon oxide (Si–O–Si vibrational band around 1100 cm^{-1}) and some silanol groups (Si–OH vibrational band around 3500 cm^{-1}). This oxidation technique was chosen because of its ability to generate a stable surface. Indeed, ozone-oxidized porous Si samples have been found to be stable on storage in air and on exposure to alcohols, esters, ketones and aromatics in both liquid and gas phase. All the experiments reported here were reversible, indicating that no chemical reaction between the surface and the adsorbed molecules occurs.

After preparation, the porous Si samples were mounted in a glass chamber connected to the manifold of a Schlenk line[22] that also had a flask of freeze–pump–thaw degassed solvent, a vacuum pump (Leybold Trivac), and a pressure gauge (MKS Baratron) attached. Reflectivity spectra were acquired through the glass window of the sample chamber with a bifurcated optic fiber connected on one end to a tungsten lamp and on the other end to a charge coupled device (CCD) spectrometer from Ocean Optics, Inc. Both illumination of the surface and detection of the reflected light were performed

[*] Prof. M. J. Sailor, Dr. S. E. Létant
University of California at San Diego
Department of Chemistry and Biochemistry
9500 Gilman Drive, La Jolla, CA 92093-0358 (USA)
E-mail: msailor@ucsd.edu

[**] The authors thank Dr. Daniel Derr for critical reading of the manuscript. Financial support was provided by the National Science Foundation (DMR-97-00202) and through DARPA's Tactical Sensors Program via a Space and Naval Warfare Systems Center Contract (N66001-98-C-8514). The technical point of contact for this DARPA program is Dr. Edward Carapezza.

  0935-9648/01/0503-0335 $ 17.50+.50/0